

Generation and Stabilization of Small Platinum Clusters Pt_n inside a Metal-Organic Framework

Kathrin Kratzl, Tim Kratky, Sebastian Günther, Ondrej Tomanec, Radek Zbořil, Jan Michališka, Jan M. Macák, Mirza Cokoja, and Roland A. Fischer

J. Am. Chem. Soc., **Just Accepted Manuscript** • DOI: 10.1021/jacs.9b07083 • Publication Date (Web): 09 Aug 2019

Downloaded from pubs.acs.org on August 10, 2019

Just Accepted

“Just Accepted” manuscripts have been peer-reviewed and accepted for publication. They are posted online prior to technical editing, formatting for publication and author proofing. The American Chemical Society provides “Just Accepted” as a service to the research community to expedite the dissemination of scientific material as soon as possible after acceptance. “Just Accepted” manuscripts appear in full in PDF format accompanied by an HTML abstract. “Just Accepted” manuscripts have been fully peer reviewed, but should not be considered the official version of record. They are citable by the Digital Object Identifier (DOI®). “Just Accepted” is an optional service offered to authors. Therefore, the “Just Accepted” Web site may not include all articles that will be published in the journal. After a manuscript is technically edited and formatted, it will be removed from the “Just Accepted” Web site and published as an ASAP article. Note that technical editing may introduce minor changes to the manuscript text and/or graphics which could affect content, and all legal disclaimers and ethical guidelines that apply to the journal pertain. ACS cannot be held responsible for errors or consequences arising from the use of information contained in these “Just Accepted” manuscripts.

Generation and Stabilization of Small Platinum Clusters $Pt_{12\pm x}$ Inside a Metal-Organic Framework

Kathrin Kratzl,^a Tim Kratky,^a Sebastian Günther,^a Ondřej Tomanec,^b Radek Zbořil,^b Jan Michalička,^c Jan M. Macak,^c Mirza Cokoja,^a Roland A. Fischer^{a,*}

^a Catalysis Research Center, Technical University of Munich, 85748 Garching, Germany

^b Regional Center of Advanced Technologies and Materials, 78371 Olomouc, Czech Republic

^c Central European Institute of Technology, 61200 Brno, Czech Republic

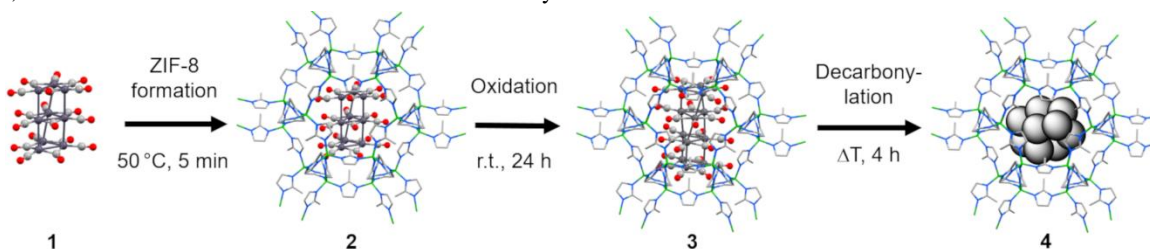
Atom-precise clusters, metal-organic framework, metal@MOF, hydrogenation catalysis, platinum nanoparticles

ABSTRACT: The generation and matrix stabilization of ligand-free, small platinum nanoclusters (NCs) $Pt_{12\pm x}$ is presented. The metal-organic framework-template approach is based on encapsulating CO-ligated, atom-precise Pt_9 Chini clusters $[\{Pt_3(CO)_6\}_3]^{2-}$ into the zeolitic imidazolate framework ZIF-8. The selective formation of the air-stable inclusion compound $[NBu_4]_2[\{Pt_3(CO)_6\}_4]@ZIF-8$ of defined atomicity Pt_{12} and with Pt loadings of 1-20 wt.% was monitored by UV/Vis and IR spectroscopy and was confirmed by high resolution transmission electron microscopy (HR-TEM), high-angle annular dark-field scanning transmission electron microscopy (HAADF-STEM), X-ray photoelectron spectroscopy (XPS) and powder X-ray diffraction (PXRD). Thermally induced decarbonylation at 200 °C yields the composite material $Pt_n@ZIF-8$ with a cluster atomicity n close to 12, irrespective of the Pt loading. The PtNCs retain their size even during annealing at 300 °C for 24 h and during catalytic hydrogenation of 1-hexene at 25 °C in liquid phase. The $Pt_n@ZIF-8$ material can conveniently be used for storing small PtNCs and their further processing. Removal of the protective ZIF-8 matrix under acidic conditions and transfer of the PtNCs to carbon substrates yields defined aggregation to small Pt nanoparticles (1.14 ± 0.35 nm, HR-TEM), which have previously shown exceptional performance in the electrocatalytic oxygen reduction reaction (ORR).

INTRODUCTION

Much research has been devoted to the study of the size effects of metal particles in catalysis, from small 2-5 nm sized nanoparticles down to ultrasmall nanoparticles and atom precise clusters consisting of less than 50 atoms.¹⁻³ Studies have shown that the reactivity not only depends on the nanoparticle size and on the surface to volume ratio, but that – approaching the sub-nanometer level – the exact atomicity (nuclearity, n) of the metal cluster becomes decisive, as “every atom counts” in this regime.⁴⁻⁶ This has been attributed to unique cluster structures, isomers and structural fluctuations leading to distinct electronic properties, special surface sites and defects with altered, and even enhanced reactivity.^{7,8}

Therefore, the desire is to develop synthetic approaches for ligand-free metal clusters with a precise number of metal atoms, so as to optimize the catalytic activity on an atomic level.^{9,10} While preparative solution chemistry already offers synthetic concepts and a vast library of defined molecular ligand-stabilized cluster compounds, the access to non-ligated clusters is far more intricate and limited due to their extreme tendency to agglomeration.^{11,12} Even upon deposition on supports, cluster agglomeration is a very common phenomenon during catalysis or at moderately elevated temperatures.^{13,14} Rigorous synthetic methods to obtain non-ligated (naked) clusters M_n with precise control of the



Scheme 1. Synthesis of precise PtNCs in ZIF-8. The Chini cluster $[NBu_4]_2[\{Pt_3(CO)_6\}_3]$ (1) is encapsulated in ZIF-8 to yield the composite material $[NBu_4]_2[\{Pt_3(CO)_6\}_3]@ZIF-8$ (2). Oxidation of 2 leads to formation of $[NBu_4]_2[\{Pt_3(CO)_6\}_4]@ZIF-8$ (3). The decarbonylation of 3 at 200 °C provides naked PtNCs, denoted as PtNC@ZIF-8 (4).

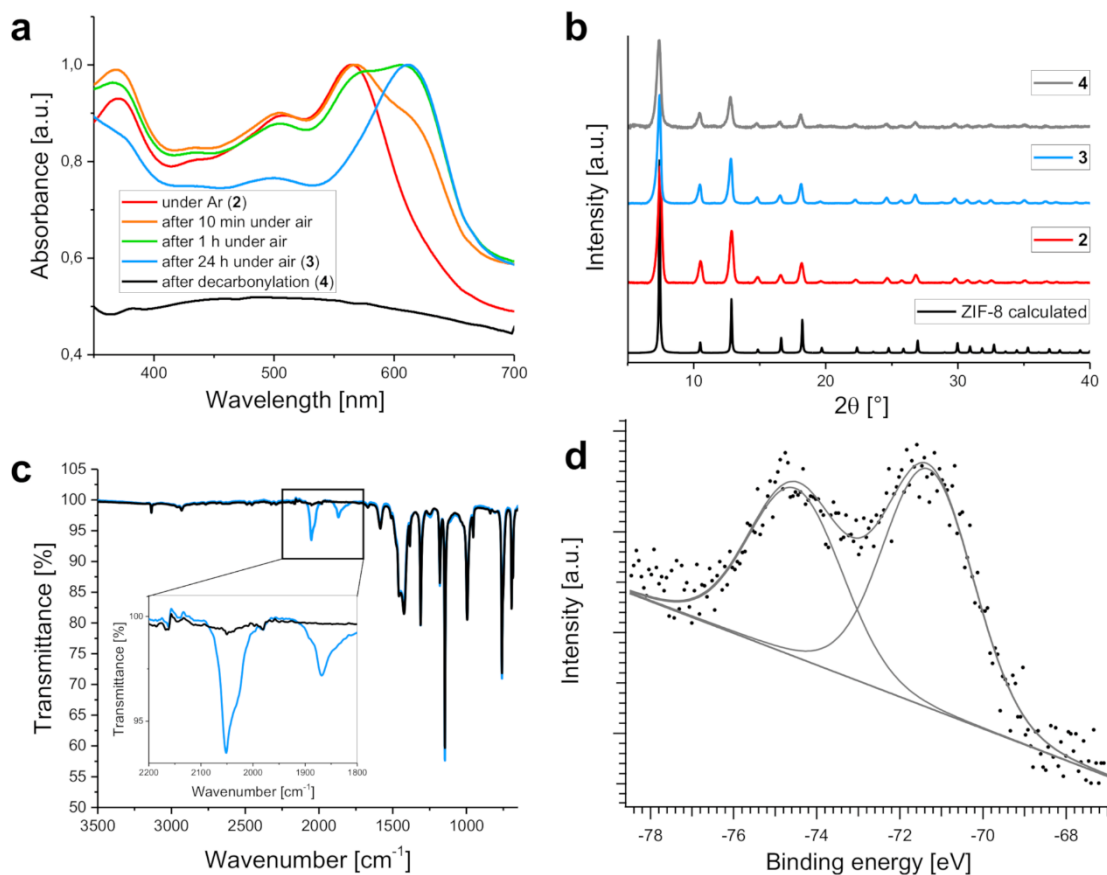


Figure 1. (a) Solid-state UV/Vis spectra of **2-4** with slowed-down oxidation by sample sealing with silicon grease. While the band characteristic for **2** (562 nm) disappears during oxidation, the band for **3** (620 nm) increases and shows no shoulders for the next larger Pt₁₅ cluster (702 nm). After decarbonylation, no bands are visible for **4**. (b) PXRD patterns of **2-4** compared to the calculated pattern of ZIF-8 ($\lambda=1.5406$ Å). The ZIF matrix is highly crystalline throughout all reaction steps and it was possible to reproduce the patterns multiple times. (c) Comparative FT-IR spectra of **3** (blue) and **4** (black). After heating under vacuum, the CO bands for terminal (2051 cm^{-1}) and bridging (1868 cm^{-1}) CO ligands (inset) completely disappeared, confirming full decarbonylation. (d) XP spectrum of the Pt 4f region of **4**.

atomicity “n” rely on sophisticated and expensive methods like e.g. laser ablation techniques¹⁵ under isolated conditions, or on dendrimer-based nanoreactor-template approaches in solution.¹⁶

Metal-organic frameworks (MOFs) have been recognized and widely studied as uniquely versatile and tunable matrices and porous support materials, to encapsulate catalytically active metal nanoparticles^{17–21} and we were pioneers in this field as early as in 2005.²² Often, however, encapsulation of nanoparticles in MOFs does not bring much additional benefit, but diffusion limitations hamper the catalytic activity of the “metal@MOF” heterogeneous catalyst as compared to homogeneous reference systems.^{23,24} Nevertheless, loading or post-synthetic modification of MOFs with catalytically active metal/metal-oxide species by various techniques has developed into an important research field. In particular, the application of atomic layer deposition (ALD) techniques inside MOFs, called AIM and introduced by J. T. Hupp, has opened new perspectives.²⁵ However, the precise control of atomicity of metal clusters M_n encapsulated, deposited or grown inside MOFs (or any other porous matrix) is still a huge challenge, and among the very few reports that include catalytically

relevant metals are the ultrasmall clusters Pd₄ or Pt₂ which were generated inside specifically designed MOFs.^{26,27} In contrast to the direct growth of non-ligated metal clusters (or nanoparticles) inside MOFs through decomposing molecular precursors,^{17–27} the encapsulation of preformed atom-precise and ligand stabilized metal clusters $[M_nL_m]$ into MOFs has not been studied in detail, and to the best of our knowledge only one example has been reported using the gold cluster $[Au_{25}(SG)_{18}]$ (SG = glutathionate, γ -L-Glutamyl-L-cysteinyl-glycinate) and the zeolitic imidazolate framework ZIF-8 as the host.²⁸ It is as yet unknown whether a selective deprotection of a ligated cluster $[M_nL_m]$ to yield the non-ligated M_n cluster inside the cavities of the MOF is feasible without extensive agglomeration and loss of control of cluster atomicity.

In this work we demonstrate proof-of-concept by the “bottle-around-ship” synthesis of the inclusion compound $[NBu_4]_2\{[Pt_3(CO)_6]_4\}@ZIF-8$ and the subsequent thermal decarbonylation to yield ultrasmall Pt_{12±x} nanoclusters (NCs) uniformly distributed in the pores of the ZIF-8 matrix. The clusters retain their size even during annealing at 300 °C for 24 h and during catalytic hydrogenation of 1-hexene at 25 °C in liquid phase.

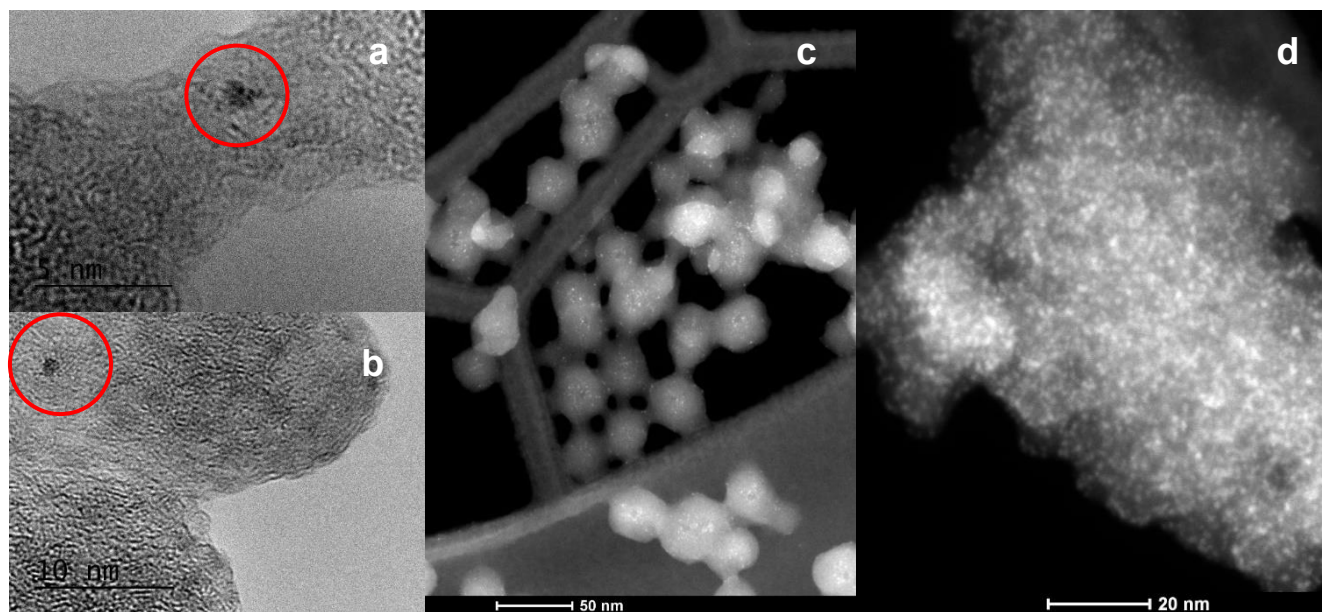


Figure 2. Microscopic images of **3** and **4**. (a) HR-TEM image of a single PtNC in **3**. Scale bar is 5 nm. (b) HR-TEM image of a single PtNC in **4**. Scale bar is 10 nm. (c) HAADF-STEM image of **4**. PtNCs are visible as bright dots. No agglomerated nanoparticles are visible even after decarbonylation. (d) HAADF-STEM image of **3-max**. PtNCs are visible as small bright dots, showing the stabilization of the PtNCs in the MOF that prevents agglomeration even upon close proximity of naked metal clusters.

The material Pt₉@ZIF-8 can conveniently be used for storing ultrasmall PtNCs and for further processing such as fabrication of high performing electrocatalysts for the oxygen reduction reaction (ORR).

RESULTS and DISCUSSION

Synthesis and Characterization of [NBu₄]₂[Pt₃(CO)₆]₄@ZIF-8. The red-colored Pt₉ Chini cluster compound [NBu₄]₂[Pt₃(CO)₆]₃ (**1**) was chosen as a representative example of the vast family of atom-precise carbonyl metallate clusters of the general formula [M_a(CO)_b]^{k-} (M also includes mixed metals).^{29,30} Its synthesis is comparably facile³¹ and its characterization and the distinction of [Pt₃(CO)₆]₃²⁻ (Pt₉) from the series of related clusters [Pt₃(CO)₆]_n²⁻ (e.g. Pt₁₂, Pt₁₅ etc.) is very sensitive and unambiguous via UV/Vis and IR spectroscopy (Figures S1 and S2 in the Supporting Information, SI).³² As a supporting MOF, we selected a zeolitic imidazolate framework, namely [Zn(2-methylimidazolate)₂] (ZIF-8) because of its mild synthesis conditions in solution and its high thermal stability (up to 500 °C), which is important for the planned thermal decarbonylation procedure and long-term annealing studies.³³

Microporous ZIF-8 exhibits small, cage-like pores (11.6 Å) as well as small pore windows (3.4 Å, static conditions) that are expected to restrict the mobility of the encapsulated clusters and prevent agglomeration.³⁴ The targeted Pt₁₂ NCs exhibit a Van der Waals radius of 9±1 Å – as reported in dendrimers by Imaoka³⁵ – which exceeds the diameter of the pore opening even when considering the flexibility of ZIF-8.³⁶ It should be noted that the size distribution of 1 Å is due to the error in size determination from HR-TEM pictures, although the clusters have been shown to be atom-precise. The Pt₁₂ NCs

should thus be small enough to fit into the pore of ZIF-8 but be completely immobilized due to their inability to pass through the pore opening. The encapsulation of **1** was carried out at 50 °C in methanol solution under inert conditions (dry Ar atmosphere) in the presence of zinc nitrate and 2-methylimidazole as the components for the self-assembly of the ZIF-8 (see Scheme 1). The obtained red, oxidation-sensitive inclusion compound [NBu₄]₂[Pt₃(CO)₆]₃@ZIF-8 (**2**) contains the intact Pt₉ Chini cluster **1**, as confirmed by UV/Vis, IR and microscopic measurements. Upon exposition of **2** to air at ambient conditions, the color of the material gradually changes within 10 min to blue, indicating the formation of [NBu₄]₂[Pt₃(CO)₆]₄@ZIF-8 (**3**), which matches the color of the independently synthesized Pt₁₂ Chini cluster compound [NBu₄]₂[Pt₃(CO)₆]₄ (Figure S3). The transformation of **2** to **3** was monitored via solid state UV/Vis (Figure 1a). Chini clusters are known to be easily transformed into complex mixtures of larger clusters, depending on the oxidizing conditions, by the exchange of growth units {Pt₃(CO)₆} resulting in fast degradation of smaller clusters.^{32,37} In contrast to this well-known redox-chemistry in solution, the oxidation of the Pt₉ cluster inside ZIF-8 was selective and the formation of the Pt₁₂ compound **3** was quantitative as judged by UV/Vis spectroscopy. The cluster was even intact after one day in boiling water or 1M sodium hydroxide solution, under which conditions the ‘free’ cluster immediately decomposes in solution (Figure S4). The sensitivity of **2** towards oxygen in contrast to the stable **3** can be explained with a remaining mobility of the Pt₉ carbonyl cluster in ZIF-8, so that {Pt₃(CO)₆} fragments can be transferred upon oxidation as it has been reported for the Chini clusters in solution.³⁷ In contrast, the resulting Pt₁₂ carbonyl cluster fills the volume of the narrow ZIF-8 pore and its even larger oxidation product Pt₁₅ cannot be accomo-

dated. This fact was also used to compensate for eventual Pt₉/Pt₁₂ mixtures which were observable in some of the encapsulation experiments. The high excess of basic imidazole induced an oxidation of the Pt₉ cluster unless it was rapidly encapsulated and protected inside the ZIF-8 matrix. Because of these competing kinetics of ZIF crystal formation and the redox chemistry of the cluster, conditions were tuned towards a rapid crystallization and encapsulation process. This resulted in weakly faceted, partially intergrown ZIF-8 particles with diameters that slightly varied from batch to batch. The Pt loading is easily tunable by variation of the amount of Pt₉ added during the reaction.

Powder X-ray diffraction (PXRD) confirmed the high crystallinity of the ZIF-8 matrix (Figure 1b). Nitrogen adsorption experiments showed a high porosity that varied with Pt loading due to the increase of non-porous mass. The obtained values are in the range of literature values for the internal surface area of ZIF-8 (1630 m²/g) (Figure S5).³⁸

Decarbonylation and Characterization of Pt_{12±x}@ZIF-8.

Previous studies with Chini clusters in zeolites and porous silica revealed that the carbonyl ligands quantitatively dissociate at elevated temperatures.^{39,40} In-situ IR spectroscopic studies demonstrate that the decarbonylation process of **3** starts around 140 °C and is completed after 15 min at 200 °C. The total loss of CO is evidenced by the complete disappearance of both bands for the terminal as well as for the bridging CO ligands (Figure 1c, Figure S7). In this respect, **3** is heated at 200 °C under vacuum for four hours, to ensure complete decarbonylation of the clusters. This process can be also followed via thermogravimetric analysis (TGA), where an initial step corresponds to the weight loss due to ligand removal (Figure S8). At higher loadings of Pt₉, the extent of this initial weight loss increases as more carbonyl ligands are lost at elevated temperatures. In the decarbonylated material, the first weight loss step is absent, validating the decarbonylation conditions that apparently are able to remove all carbonyl ligands. In an in-situ XPS experiment, **4** was obtained by oxidation of **2** in 200 mbar O₂ at room temperature overnight and subsequent decarbonylation in vacuum ($\leq 10^{-6}$ mbar) at 200 °C for 3 hours in a preparation chamber attached to the XPS analysis chamber. We do not present any XP spectra of **2** and **3**, as we observed significant beam damage even with lowest X-ray flux, most likely leading to decarbonylation of the PtNCs. It has been reported in the literature that, in particular, supported Pt Chini clusters are prone to decarbonylation while illuminating with X-rays.^{41–43} One pair of spin-orbit split peaks is used to deconvolute the rather weak and broad Pt 4f photoelectron signal. The binding energy of 71.1 eV (Pt 4f_{7/2}) is close to that reported for decarbonylated PtNCs (Figure 1d). Zn 2p and N 1s signals coincide with ZIF-8 spectra reported in literature (Figure S9).^{44,45}

The ZIF-8 matrix retains its crystallinity and porosity as evidenced in PXRD and nitrogen adsorption (Figure 1b, Figure S6) while in UV/Vis, no bands are discernible anymore (Figure 1a). The latter is because of an expected cluster rearrangement and a collapse of the layered structure after ligand dissociation, which causes the absence of the respective electronic transitions. The obtained material Pt_n@ZIF-8 (**4**) was further characterized by HR-TEM microscopy and HAADF-

STEM with elemental mapping. The data show a PtNC diameter of ca. 1 nm consistent with previously reported Pt₁₂ clusters³⁵ and indicate that the decarbonylated clusters Pt_n are stabilized towards agglomeration and are homogeneously distributed throughout ZIF-8 (Figure 2, Figures S10 and S11). Annealing studies of **4** at 300 °C for 24 h revealed no changes and the material remained intact as evidenced by PXRD and HAADF-STEM (Figure S12). We deliberately refrain from showing size distribution histograms due to the high error in cluster atomicity determination for the size regime around 1 nm inside the ZIF-8 host matrix. Higher resolutions to obtain a suitable accuracy for conclusive determination of PtNC diameters (aiming at atomic resolution) are extremely difficult to achieve and the significance of the data is limited due to the high instability of ZIF-8 under the electron beam that destroyed the framework upon longer exposure (see Figure S13).⁴⁶ Nonetheless, when comparing HR-TEM images of the material **3** before decarbonylation with material **4** after decarbonylation, no obvious changes in cluster size distribution are observable. Based on the available analytical methods and resolutions, the exact atomicity and distribution of nuclearities of the small PtNCs cannot be determined. Still, we can exclude a significant degree of sintering based on HR-TEM and HAADF-STEM pictures, suggesting a good stabilization of the Pt₁₂ NCs even after decarbonylation. Thus, available data indicates the presence of Pt_{12±x} NCs inside ZIF-8 with a small uncertainty in the range of few atoms.

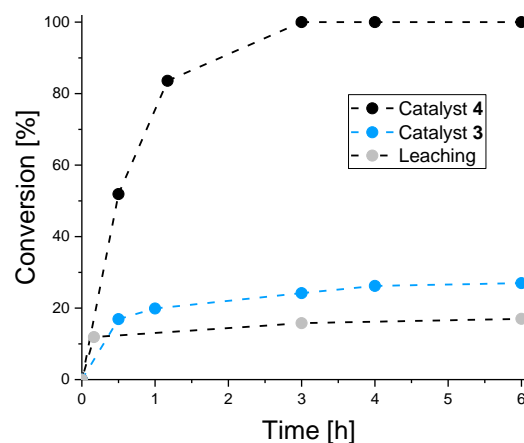


Figure 3: Catalytic hydrogenation of 1-hexene with **3** and **4** as catalysts. While with **4**, complete conversion is reached after 3 h, the ligand-stabilized clusters in **3** show a significantly slower conversion towards a steady state. When the catalyst **4** is separated after 10 min in a hot filtration experiment, only minimal further conversion is observed, presumably due to Pt species in solution.

In order to further exclude migration and aggregation effects of the clusters within the matrix, we drastically increased the loading of **1** inside ZIF-8. In the standard experiments, the loading was mostly kept low with ca. 1 wt.%. Using an excess of **1** during the ZIF-8 self-assembly, a maximum loading of 21 wt.% Pt was achieved (**3-max**). This loading corresponds to about 44% cluster pore filling (for details of the calculation, see Supporting Information).

Even at this high loading, the Pt₁₂ Chini cluster was exclusively and quantitatively formed and stayed intact, as shown via solid-state UV/Vis. The unchanged matrix was confirmed by the characteristic reflections of ZIF-8, as observed in PXRD (Figure S14). Nitrogen sorption measurements revealed an internal surface area of 670 m²/g, demonstrating the residual but severely decreased porosity of the material due to the high number of defects, which is also obvious from a lower reflection intensity in PXRD. Additionally, an increase in non-porous mass and pore filling at higher cluster loadings lowers the BET surface area.

The dense packing of the Pt₁₂ Chini clusters becomes evident through HR-TEM and HAADF-STEM and we highlight that no agglomerates were found despite the high cluster density (Figure 2d and Figure S15). Since the decarbonylation of the dianionic Pt₁₂ Chini cluster **3** under vacuum at elevated temperatures leads to neutral and naked Pt_{12±x} NCs which feature Pt(0), as shown by XPS, a redox process must be considered and characterized. We investigated the fate of the tetrabutylammonium counter ions for which a decomposition to trialkylamines at high temperatures has been reported.⁴⁷ Using the highly loaded material **3-max**, a signature of this decomposition was observed in TGA-MS (Figure S16). A similar study was conducted by Sadakiyo et al., who introduced NBu₄OH in ZIF-8.⁴⁷ While in our work, a butyl cation (m/z = 57 a.m.u.) of the NBu₄⁺ decomposition was detected at 235 °C, Sadakiyo et al. reported NBu₄⁺ decomposition as low as at 127 °C. We attribute this difference to the low amount of tetrabutylammonium cations compared to the masses of ZIF and clusters, which results in diffusion limitations and a need for higher temperatures for desorption from the MOF and thus for detection. The oxidation of the cluster upon ligand removal could be explained by exposure to oxygen or by a redox reaction with the decomposing cation. Under the decarbonylation conditions in the synthesis of **4**, NBu₄⁺ decomposition products like NBu₃ are likely removed under high vacuum (1·10⁻³ mbar). Because the absence of the amine side-product of the decomposition is difficult to prove due to the high nitrogen content of ZIF-8, the experiment was repeated with tetrabutylphosphonium as a counterion of the Chini cluster **1**. As expected, in **3** a small content of phosphorus is found by elemental analysis, stemming from PBu₄⁺ (0.04 wt.%), while in the decarbonylated material **4**, all phosphorus species are removed (0.00 wt.%) because of evacuation at high temperatures that cause the decomposition and desorption of tributylphosphine, PBu₃.

Catalytic Hydrogenation. For a proof of synthetic feasibility, and for reasons of applicability in catalysis, we have scaled up the synthesis to yield 1.80 g of **3** with a Pt loading of 1 wt.% for both **3** and **4**. The limiting factor for further scale-up is not the encapsulation procedure of **1** to ZIF-8, but the

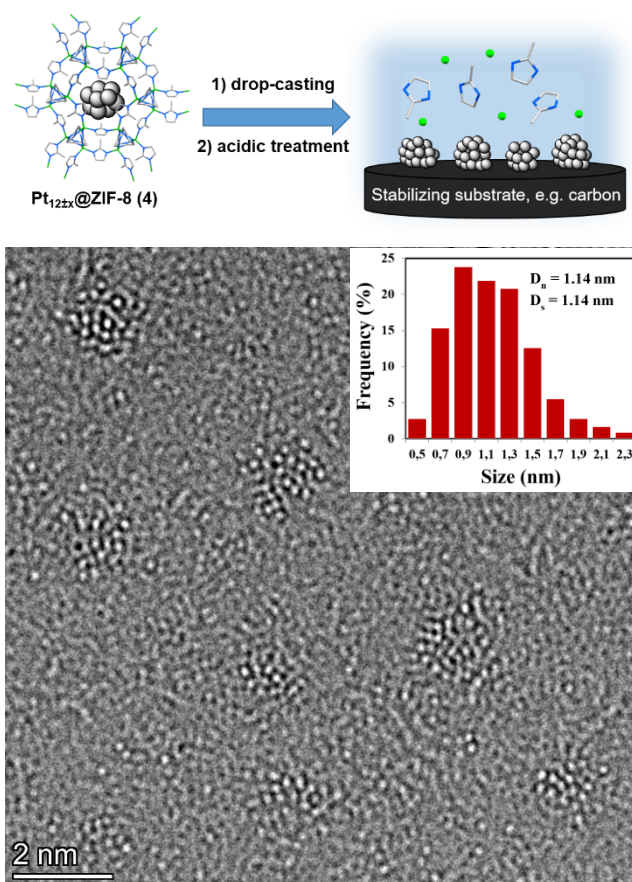


Figure 4: *Top:* Drop-casting of **4** on a stabilizing substrate and dissolution of the ZIF by protonation in acidic media yields small Pt nanoparticles. *Bottom:* HR-TEM image of **4** on a carbon-coated TEM grid after immersion in 1M HClO₄ with resulting nanoparticles of 1.14±0.35 nm for the number and surface averaged diameter (D_n and D_s, respectively) (size distribution histogram shown in inset).

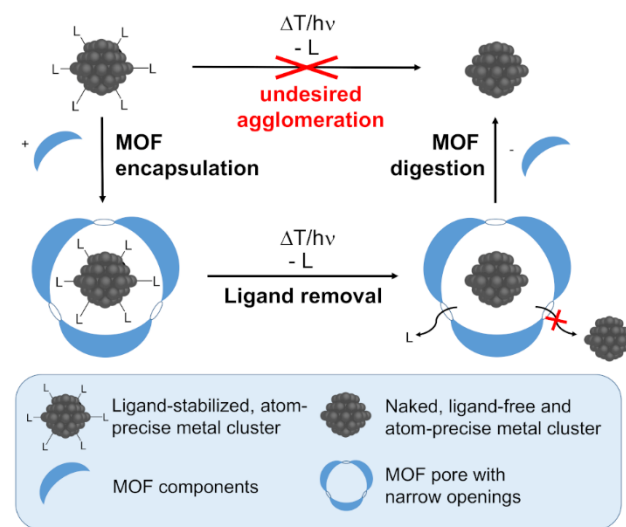
synthesis of **1**, which is time consuming and requires synthesis under CO atmosphere and work-up under inert conditions. Interestingly, the synthesis works even better at a large scale because no Pt₉/Pt₁₂ cluster mixtures were detected, in contrast to some small-scale encapsulation experiments. The catalytic potential of **4** was demonstrated in a model case study of the hydrogenation of 1-hexene. When a suspension of **4** (1 mol%; 1 wt.% Pt) with 1-hexene in toluene is treated with H₂ (1.5 bar) at room temperature, full conversion to hexane is observed within 3 h with a TOF of around 2000 h⁻¹. With the still carbonylated material **3** as the catalyst, only 24% conversion is achieved after the same period of time (Figure 3, Figure S17). This observation confirms that the removal of the carbonyl ligands to yield **4** increases the accessibility and/or abundance of active Pt sites and thus boosts the catalytic activity. The few accessible sites in **3** are rapidly saturated by solvent and/or product molecules and the reaction approaches the steady state after a short reaction time. Cyclooctene was also applied under the same hydrogenation conditions as 1-hexene with **4** as the catalyst. In contrast to the very fast and complete

conversion of the latter, cyclooctene showed only 23% conversion after a prolonged reaction time of 24 h, demonstrating that exclusively substrates which are small enough to penetrate the MOF pores can be converted efficiently. The remaining activity is attributed to leaching or Pt NCs near the external surface of the ZIF-8 crystallites that could be accessible also for bulkier substrates (Figure S18). In a hot filtration test, catalyst **4** was removed in the initial phase of high activity after 10 min by syringe-filtration (PTFE, 0.2 μm) combined with centrifugation. Only minimal conversion was observed upon re-adding hydrogen pressure, which could stem from incomplete catalyst removal due to the small ZIF-8 crystallites that are neither retained by the syringe filter nor completely separated by centrifugation, or a small amount of leached Pt species from surface-near NCs (Figure 3). Thus, it could be shown that the clusters in Pt_{12±x}@ZIF-8 and not solubilized Pt compounds are the catalytically active species. The structural integrity of the catalysts **3** and **4** was investigated after the hydrogenation reactions. Remarkably, the solid-state UV/Vis spectrum of catalyst **3** was identical to the one before the catalysis, proving the integrity of most carbonyl clusters inside the MOF even after catalysis (Figure S19). For both **3** and **4**, the PXRD patterns showed no loss in crystallinity after the hydrogenation (Figure S20).

HR-TEM and HAADF-STEM imaging as well as XPS after catalytic testing confirmed that no agglomeration had taken place (Figures S21 and S22). The integrity of the catalyst was further indicated by recycling experiments. Material **4** was recycled ten times and again showed complete conversion of 1-hexene after every recycling and activation step. In summary, the Pt_{12±x} NCs hosted by ZIF-8 show good stability in hydrogenation reactions, where many other Pt species on various other (porous) supports have been reported to show significant agglomeration and deactivation.^{43,48}

Fabrication and Microstructural Characterization of an ORR Catalyst. The presented Pt_{12±x}@ZIF-8 material serves as an excellent source of ultrasmall Pt nanoparticles upon dissolution of the stabilizing framework. This was shown previously with the synthesis of a highly active catalyst for the oxygen reduction reaction (ORR).⁴⁹ As ZIF-8 is known to form stable dispersions in methanol, **4** can be easily drop-casted onto a carbon electrode and upon immersion in the acidic electrolyte (1M HClO₄), characteristic Pt features emerge in cyclic voltammetry after 90 potential cycles.⁴⁹ During this initial period, the imidazolate linkers of ZIF-8 are protonated and the framework gradually dissolves and releases the Pt nanoclusters onto the carbon support (Figure 4). This preparation method under ambient conditions would not be feasible for the carbonyl-stabilized Chini cluster [NBu₄]₂{[Pt₃(CO)₆]₄} alone, due to its high oxidation sensitivity, resulting in uncontrolled cluster growth and disintegration. Equally, no characteristic Pt features and thus no oxygen reduction activity is observed in an alkaline medium as the Pt clusters are protected in the non-conductive ZIF matrix. This demonstrates that the slow removal of the insulating ZIF-8 is crucial to reveal the high ORR activity of small Pt species. To visualize the obtained products, the same drop-casting method is applied to a carbon-coated TEM grid with subsequent acidic treatment. HR-TEM images reveal Pt nanoparticles with a narrow size distribution

of 1.14±0.35 nm (Figure 4). Apparently, the slow dissolution of the ZIF matrix in diluted acid releases the Pt_{12±x} clusters in a controlled fashion, resulting in a surprisingly effective control of the agglomeration in parallel to the anchoring and stabilization of the PtNCs on the carbon support. This is of special importance, because exceptionally high activity has been reported for atom-precise PtNCs below 50 atoms.⁸ Getting close to such catalyst species in the most precise way possible is a major goal for rational catalyst design, and our material constitutes a significant step in this direction. Thus, Pt_{12±x}@ZIF-8 represents a “container” for sub-nanometer Pt clusters that are readily released and could be deposited onto a variety of substrates with sufficient stabilization. Looking at the broad scope of reactions with Pt-containing catalysts, the high-precision Pt nanoparticles available from Pt_{12±x}@ZIF-8 will be of high interest for the optimization of catalytic processes.



Scheme 2: General concept for the synthesis of ligand-free, atom-precise metal clusters and ultrasmall metal nanoparticles, based on the encapsulation of ligated metal clusters into size matching pores of Metal-Organic Frameworks chosen as removable protective matrix.

CONCLUSION

We present the spatial confinement of ultrasmall metal clusters in the pores of a MOF, which effectively prevents cluster agglomeration even after ligand removal. The synthesis and characterization of a novel PtNC@ZIF-8 material containing high-precision Pt nanoclusters of an atomicity near twelve is reported. PtNC@ZIF-8 acts as an excellent source for ultrasmall Pt nanoparticles since the MOF scaffold is readily dissolved under acidic conditions with minimal agglomeration on a provided support. Therefore, our synthetic concept could be transferred to a broad scope of organometallic clusters and MOFs with the prerequisite of sufficient cluster stability and rather mild MOF synthesis conditions (Scheme 2). A variety of nanomaterials would thus be accessible, displaying high stability, scalability and ease of handling, and giving a simpli-

1 fied access to highly active metal catalysts in a size range
2 close to or even below 1 nm.

3 ASSOCIATED CONTENT

4 The Supporting Information is available free of charge on the
5 ACS Publications website.

6 Information on materials, synthetic procedures, measurements,
7 additional characterizations (photographs, UV/Vis, IR, XPS,
8 TGA, HR-TEM, HAADF-STEM, PXRD, NMR) (PDF)

9 AUTHOR INFORMATION

10 Corresponding Author

11 * roland.fischer@tum.de

12 Notes

13 The authors declare no competing financial interests.

14 ACKNOWLEDGMENT

15 This work has been supported by the Deutsche Forschungsge-
16 meinschaft (DFG) via the cluster of excellence e-conversion
17 (www.e-conversion.de; EXC 2089). The authors gratefully
18 acknowledge the support by the Operational Programme Re-
19 search, Development and Education – European Regional Devel-
20 opment Fund, Project No. CZ.02.1.01/0.0/0.0/15_003/0000416 of
21 the Ministry of Education, Youth and Sports of the Czech Repub-
22 lic. Part of the work was carried out with the support of CEITEC
23 Nano Research Infrastructure (ID LM2015041, MEYS CR, 2016–
24 2019). We would like to thank Miguel Rivera-Torrente for con-
25 ducting in-situ IR measurements.

26 REFERENCES

- 27 (1) Astruc, D.; Lu, F.; Aranzas, J. R. Nanoparticles as recyclable
28 catalysts: The frontier between homogeneous and heterogeneous
29 catalysis. *Angew. Chem. Int. Ed.* **2005**, *44*, 7852–7872.
- 30 (2) Oliver-Meseguer, J.; Cabrero-Antonino, J. R.; Domínguez, I.;
31 Leyva-Pérez, A.; Corma, A. Small gold clusters formed in solution
32 give reaction turnover numbers of 10(7) at room temperature. *Science*
33 **2012**, *338*, 1452–1455.
- 34 (3) Desireddy, A.; Conn, B. E.; Guo, J.; Yoon, B.; Barnett, R. N.;
35 Monahan, B. M.; Kirschbaum, K.; Griffith, W. P.; Whetten, R. L.;
36 Landman, U. Bigioni, T. P. Ultrastable silver nanoparticles. *Nature*
37 **2013**, *501*, 399.
- 38 (4) Heiz, U.; Sanchez, A.; Abbet, S.; Schneider, W.-D. Catalytic
39 Oxidation of Carbon Monoxide on Monodispersed Platinum Clusters:
40 Each Atom Counts. *J. Am. Chem. Soc.* **1999**, *121*, 3214–3217.
- 41 (5) Lang, S. M.; Bernhardt, T. M. Gas phase metal cluster model
42 systems for heterogeneous catalysis. *Phys. Chem. Chem. Phys.* **2012**,
43 *14*, 9255–9269.
- 44 (6) Lei, Y.; Mehmood, F.; Lee, S.; Greeley, J.; Lee, B.; Seifert, S.;
45 Winans, R. E.; Elam, J. W.; Meyer, R. J.; Redfern, P. C.; Teschner,
46 D.; Schlögl, R.; Pellin, M. J.; Curtiss, L. A.; Vajda, S. Increased silver
47 activity for direct propylene epoxidation via subnanometer size ef-
48 fects. *Science* **2010**, *328*, 224–228.
- 49 (7) Harding, D. J.; Fielicke, A. Platinum group metal clusters:
50 From gas-phase structures and reactivities towards model catalysts.
51 *Chem. Eur. J.* **2014**, *20*, 3258–3267.
- 52 (8) Imaoka, T.; Kitazawa, H.; Chun, W.-J.; Yamamoto, K. Finding
53 the Most Catalytically Active Platinum Clusters With Low Atomicity.
54 *Angew. Chem. Int. Ed.* **2015**, *54*, 9810–9815.

- (9) Jin, R. Atomically precise metal nanoclusters: Stable sizes and
optical properties. *Nanoscale* **2015**, *7*, 1549–1565.
- (10) Wilcoxon, J. P.; Abrams, B. L. Synthesis, structure and prop-
erties of metal nanoclusters. *Chem. Soc. Rev.* **2006**, *35*, 1162–1194.
- (11) Lopez-Sanchez, J. A.; Dimitratos, N.; Hammond, C.; Brett, G.
L.; Kesavan, L.; White, S.; Miedziak, P.; Tiruvalam, R.; Jenkins, R.
L.; Carley, A. F.; Knight, D.; Kiely, C. J.; Hutchings, G. J. Facile
removal of stabilizer-ligands from supported gold nanoparticles.
Nature Chem. **2011**, *3*, 551 EP -.
- (12) Wang, Y.; Su, H.; Xu, C.; Li, G.; Gell, L.; Lin, S.; Tang, Z.;
Häkkinen, H.; Zheng, N. An intermetallic Au₂₄Ag₂₀ superatom
nanocluster stabilized by labile ligands. *J. Am. Chem. Soc.* **2015**, *137*,
4324–4327.
- (13) Valden, M.; Lai, X.; Goodman, D. W. Onset of Catalytic Ac-
tivity of Gold Clusters on Titania with the Appearance of Nonmetallic
Properties. *Science* **1998**, *281*, 1647–1650.
- (14) Cheng, N.; Stambula, S.; Wang, D.; Banis, M. N.; Liu, J.;
Riese, A.; Xiao, B.; Li, R.; Sham, T.-K.; Liu, L.-M.; Botton, G. A.;
Sun, X. Platinum single-atom and cluster catalysis of the hydrogen
evolution reaction. *Nature Comm.* **2016**, *7*, 13638 EP -.
- (15) Schweinberger, F. F.; Berr, M. J.; Döblinger, M.; Wolff, C.;
Sanwald, K. E.; Crampton, A. S.; Ridge, C. J.; Jäckel, F.; Feldmann,
J.; Tschurl, M.; Heiz, U. Cluster size effects in the photocatalytic
hydrogen evolution reaction. *J. Am. Chem. Soc.* **2013**, *135*, 13262–
13265.
- (16) Imaoka, T.; Kitazawa, H.; Chun, W.-J.; Omura, S.; Albrecht,
K.; Yamamoto, K. Magic number Pt₁₃ and misshapen Pt₁₂ clusters:
Which one is the better catalyst? *J. Am. Chem. Soc.* **2013**, *135*,
13089–13095.
- (17) Moon, H. R.; Lim, D.-W.; Suh, M. P. Fabrication of metal na-
noparticles in metal-organic frameworks. *Chem. Soc. Rev.* **2013**, *42*,
1807–1824.
- (18) Esken, D.; Turner, S.; Lebedev, O. I.; van Tendeloo, G.;
Fischer, R. A. Au@ZIFs: Stabilization and Encapsulation of Cavity-
Size Matching Gold Clusters inside Functionalized Zeolite Imidazo-
late Frameworks, ZIFs. *Chem. Mater.* **2010**, *22*, 6393–6401.
- (19) Dhakshinamoorthy, A.; Garcia, H. Catalysis by metal nano-
particles embedded on metal-organic frameworks. *Chem. Soc. Rev.*
2012, *41*, 5262–5284.
- (20) White, R. J.; Luque, R.; Budarin, V. L.; Clark, J. H.; Macquar-
rie, D. J. Supported metal nanoparticles on porous materials. Methods
and applications. *Chem. Soc. Rev.* **2009**, *38*, 481–494.
- (21) Rösler, C.; Fischer, R. A. Metal-organic frameworks as hosts
for nanoparticles. *CrystEngComm* **2015**, *17*, 199–217.
- (22) Hermes, S.; Schröter, M.-K.; Schmid, R.; Khodeir, L.; Muhler,
M.; Tissler, A.; Fischer, R. W.; Fischer, R. A. Metal@MOF: Loading
of highly porous coordination polymers host lattices by metal organic
chemical vapor deposition. *Angew. Chem. Int. Ed.* **2005**, *44*, 6237–
6241.
- (23) Hermannsdörfer, J.; Friedrich, M.; Kempe, R. Colloidal size
effect and metal-particle migration in M@MOF/PCP catalysis. *Chem-
istry* **2013**, *19*, 13652–13657.
- (24) Lu, G.; Li, S.; Guo, Z.; Farha, O. K.; Hauser, B. G.; Qi, X.;
Wang, Y.; Wang, X.; Han, S.; Liu, X.; DuChene, J. S.; Zhang, H.;
Zhang, Q.; Chen, X.; Ma, J.; Loo, S. C. J.; Wei, W. D.; Yang, Y.;
Hupp, J. T.; Huo, F. Imparting functionality to a metal-organic
framework material by controlled nanoparticle encapsulation. *Nat.*
Chem. **2012**, *4*, 310.
- (25) Islamoglu, T.; Goswami, S.; Li, Z.; Howarth, A. J.; Farha, O.
K.; Hupp, J. T. Postsynthetic Tuning of Metal-Organic Frameworks
for Targeted Applications. *Acc. Chem. Res.* **2017**, *50*, 805–813.
- (26) Fortea-Pérez, F. R.; Mon, M.; Ferrando-Soria, J.; Boronat, M.;
Leyva-Pérez, A.; Corma, A.; Herrera, J. M.; Osadchii, D.; Gascon, J.;
Armentano, D.; Pardo, E. The MOF-driven synthesis of supported
palladium clusters with catalytic activity for carbene-mediated chem-
istry. *Nat. Mater.* **2017**, *16*, 760.

- (27) Mon, M.; Rivero-Crespo, M. A.; Ferrando-Soria, J.; Vidal-Moya, A.; Boronat, M.; Leyva-Pérez, A.; Corma, A.; Hernández-Garrido, J. C.; López-Haro, M.; Calvino, J. J.; Ragazzon, G.; Credi, A.; Armentano, D.; Pardo, E. Synthesis of Densely Packaged, Ultrasmall PtO₂ Clusters within a Thioether-Functionalized MOF: Catalytic Activity in Industrial Reactions at Low Temperature. *Angew. Chem. Int. Ed.* **2018**, *57*, 6186–6191.
- (28) Luo, Y.; Fan, S.; Yu, W.; Wu, Z.; Cullen, D. A.; Liang, C.; Shi, J.; Su, C. Fabrication of Au₂₅(SG)₁₈-ZIF-8 Nanocomposites: A Facile Strategy to Position Au₂₅(SG)₁₈ Nanoclusters Inside and Outside ZIF-8. *Adv. Mater.* **2018**, *30*, DOI: 10.1002/adma.201704576.
- (29) Zacchini, S. Using Metal Carbonyl Clusters To Develop a Molecular Approach towards Metal Nanoparticles. *Eur. J. Inorg. Chem.* **2011**, *2011*, 4125–4145.
- (30) Chini, P. Large Metal Carbonyl Clusters. *J. Organomet. Chem.* **1980**, *200*, 37–61.
- (31) Dragonetti, C.; Ceriotti, A.; Roberto, D.; Ugo, R. Surface-Mediated Organometallic Synthesis: The Role of the Oxidation State and of Ancillary Ligands in the High-Yield and Selective Syntheses of Platinum Carbonyl Dianions [Pt₃(CO)₆]ⁿ⁻ (n = 6, 5, 4, 3) by Reductive Carbonylation under Mild Conditions and in the Presence of Surface Basicity of Various Silica-Supported Pt(IV) or Pt(II) Compounds. *Organometallics* **2007**, *26*, 310–315.
- (32) Longoni, G.; Chini, P. Synthesis and chemical characterization of platinum carbonyl dianions [Pt₃(CO)₆]ⁿ⁻ (n = .apprx.10,6,5,4,3,2,1). A new series of inorganic oligomers. *J. Am. Chem. Soc.* **1976**, *98*, 7225–7231.
- (33) Cravillon, J.; Münzer, S.; Lohmeier, S.-J.; Feldhoff, A.; Huber, K.; Wiebcke, M. Rapid Room-Temperature Synthesis and Characterization of Nanocrystals of a Prototypical Zeolitic Imidazolate Framework. *Chem. Mater.* **2009**, *21*, 1410–1412.
- (34) Banerjee, R.; Phan, A.; Wang, B.; Knobler, C.; Furukawa, H.; O’Keeffe, M.; Yaghi, O. M. High-throughput synthesis of zeolitic imidazolate frameworks and application to CO₂ capture. *Science* **2008**, *319*, 939–943.
- (35) Yamamoto, K.; Imaoka, T.; Chun, W.-J.; Enoki, O.; Katoh, H.; Takenaga, M.; Sonoi, A. Size-specific catalytic activity of platinum clusters enhances oxygen reduction reactions. *Nat. Chem.* **2009**, *1*, 397–402.
- (36) Moggach, S. A.; Bennett, T. D.; Cheetham, A. K. The effect of pressure on ZIF-8: Increasing pore size with pressure and the formation of a high-pressure phase at 1.47 GPa. *Angew. Chem. Int. Ed.* **2009**, *48*, 7087–7089.
- (37) Ciabatti, I.; Femoni, C.; Iapalucci, M. C.; Longoni, G.; Zacchini, S. Platinum Carbonyl Clusters Chemistry: Four Decades of Challenging Nanoscience. *J. Clust. Sci.* **2014**, *25*, 115–146.
- (38) Park, K. S.; Ni, Z.; Côté, A. P.; Choi, J. Y.; Huang, R.; Uribe-Romo, F. J.; Chae, H. K.; O’Keeffe, M.; Yaghi, O. M. Exceptional chemical and thermal stability of zeolitic imidazolate frameworks. *Proc. Natl. Acad. Sci. U. S. A.* **2006**, *103*, 10186–10191.
- (39) Nováková, J. Removal of CO ligands from Pt anionic carbonyls in zeolites by heat treatment in vacuum or in a hydrogen atmosphere and following subsequent recarbonylation. *Phys. Chem. Chem. Phys.* **2001**, *3*, 2704–2711.
- (40) Fukuoka, A.; Higashimoto, N.; Sakamoto, Y.; Sasaki, M.; Sugimoto, N.; Inagaki, S.; Fukushima, Y.; Ichikawa, M. Ship-in-bottle synthesis and catalytic performances of platinum carbonyl clusters, nanowires, and nanoparticles in micro- and mesoporous materials. *Catal. Today* **2001**, *66*, 23–31.
- (41) Apai, G.; Lee, S. T.; Mason, M. G.; Gerenser, L. J.; Gardner, S. A. X-ray photoemission study of platinum carbonyl dianions [Pt₃(CO)₆]ⁿ⁻ (n = 2,3,4,5,6, .apprx. 10). *J. Am. Chem. Soc.* **1979**, *101*, 6880–6883.
- (42) Bhaduri, S.; Sharma, K. R. Anion exchange resin supported cluster carbonyl anions as catalysts. *Dalton Trans.* **1984**, 2309–2313.
- (43) Basu, S.; Mapa, M.; Gopinath, C.; Doble, M.; Bhaduri, S.; Lahiri, G. MCM-41-supported platinum carbonyl cluster-derived catalysts for asymmetric and nonasymmetric hydrogenation reactions. *J. Catal.* **2006**, *239*, 154–161.
- (44) Liu, S.; Chen, F.; Li, S.; Peng, X.; Xiong, Y. Enhanced photocatalytic conversion of greenhouse gas CO₂ into solar fuels over g-C₃N₄ nanotubes with decorated transparent ZIF-8 nanoclusters. *Appl. Catal. B* **2017**, *211*, 1–10.
- (45) Papporello, R. L.; Miró, E. E.; Zamaro, J. M. Secondary growth of ZIF-8 films onto copper-based foils. Insight into surface interactions. *Microporous Mesoporous Mat.* **2015**, *211*, 64–72.
- (46) Wiktor, C.; Meledina, M.; Turner, S.; Lebedev, O. I.; Fischer, R. A. Transmission electron microscopy on metal–organic frameworks – a review. *J. Mater. Chem. A* **2017**, *5*, 14969–14989.
- (47) Sadakiyo, M.; Kasai, H.; Kato, K.; Takata, M.; Yamauchi, M. Design and synthesis of hydroxide ion-conductive metal-organic frameworks based on salt inclusion. *J. Am. Chem. Soc.* **2014**, *136*, 1702–1705.
- (48) Chupas, P. J.; Chapman, K. W.; Jennings, G.; Lee, P. L.; Grey, C. P. Watching nanoparticles grow: The mechanism and kinetics for the formation of TiO₂-supported platinum nanoparticles. *J. Am. Chem. Soc.* **2007**, *129*, 13822–13824.
- (49) Garlyyev, B.; Kratzl, K.; Rück, M.; Michalička, J.; Fichtner, J.; Macak, J.; Kratky, T.; Günther, S.; Cokoja, M.; Bandarenka, A.; Fischer, R. A. Optimizing the size of platinum nanoparticles for enhanced oxygen electro-reduction mass activity. *Angew. Chem. Int. Ed.* **2019**, *58*, 9596–9600.

Graphic entry for the Table of Contents (TOC)

